Microarray analysis of PDGFRα$^+$ populations in ES cell differentiation culture identifies genes involved in differentiation of mesoderm and mesenchyme including ARID3b that is essential for development of embryonic mesenchymal cells

Atsushi Takebe [a,c], Takumi Era [a,*], Mitsuhiro Okada [a,b], Lars Martin Jakt [a,b], Yoshikazu Kuroda [c], Shin-Ichi Nishikawa [a]

[a] Laboratory for Stem Cell Biology, RIKEN Center for Development Biology, 2-2-3 Minatojima-minamimachi, Chuo-ku, Kobe, Hyogo 650-0047, Japan
[b] The Foundation for Biomedical Research and Innovation, 2-2-3 Minatojima-minamimachi, Chuo-ku, Kobe, Hyogo 650-0047, Japan
[c] Division of Gastroenterological Surgery, Graduate School of Medicine, Kobe University, 7-5-2 Kusunoki-cho, Chuo-ku, Kobe, Hyogo 650-0017, Japan

Abstract

An inherent difficulty in using DNA microarray technology on the early mouse embryo is its relatively small size. In this study, we investigated whether use of ES cell differentiation culture, which has no theoretical limit in the number of cells that can be generated, can improve this situation. Seven distinct ES-cell-derived populations were analyzed by DNA microarray and examined for genes whose distribution patterns are similar to those of PDGFRα, a gene implicated in differentiation of mesoderm/mesenchymal lineages. Using software developed in our laboratory, we formed a group of 30 genes which showed the highest similarity to PDGFRα, 18 of these genes were shown to be involved in development of either mesodermal, mesenchymal or neural crest cells. This list also contains several genes whose role in embryogenesis has not yet been fully identified. One such molecule is mARID3b. The mARID3b expression is found in the paraxial mesoderm and cranial mesenchyme. mARID3b-null mouse showed early embryonic lethality, and most phenotypes of this mutant appear to develop from a failure to generate a sufficient number of cranial mesenchymal cells. These results demonstrate the potential use of ES cell differentiation culture in identifying novel genes playing an indispensable role in embryogenesis.
© 2005 Elsevier Inc. All rights reserved.

Keywords: ES cell; In vitro differentiation; DNA microarray; PDGFRα; ARID3b

Introduction

While current mouse molecular genetics has progressed to a level in which the function of a particular gene expressed in the early embryo can be characterized to a large extent, the mouse embryo, due to its small size, remains a difficult subject in which to identify novel genes. In most cases, this has meant performing gene cloning on sources other than the actual embryo or isolating mouse homologues of genes known to play a role in the development of other species in which gene cloning is easier than in mouse embryo (Anderson and Ingham, 2003; Chen and Ekker, 2004; Gehring, 1993). Although both these alternative methods are effective in revealing the molecules underlying early mouse embryogenesis, isolating novel genes directly from mouse embryos would be of considerable use to researchers in this field.

One alternative strategy for obtaining cells corresponding to those in the mouse embryo is to use mouse embryonic stem (mES) cells (Loebel et al., 2003). As an in vitro mES cell culture can undergo unlimited growth while maintaining pluripotency, it is potentially an ideal source of a sufficient number of embryonic cells required for studies such as DNA microarray analysis. However, mES cell differentiation culture has not yet become a popular method for cloning genes involved in early embryogenesis as it still remains difficult to obtain pure

---

* Corresponding author.
  E-mail address: tera@cdb.riken.jp (T. Era).

populations from a culture of cells undergoing enormous diversification (Aubert et al., 2002; Jackson et al., 2002).

We have developed a set of surface markers that recognize various intermediate stages during differentiation of mesodermal/mesenchymal cells (Nishikawa et al., 1998). Vascular endothelial growth factor receptor 2 (VEGFR2), a receptor type tyrosine kinase, is expressed in lateral and extra-embryonic mesodermal cells at the gastrula stage (Yamaguchi et al., 1993). Our group and others have demonstrated that ES-cell-derived VEGFR2^{+} cells can give rise to both endothelial cells (ECs) and hematopoietic cells (HPCs) that are progenies of lateral and extra-embryonic mesoderms (Kabrun et al., 1997; Wang et al., 2004; Yamashita et al., 2000). This suggests that ES-cell-derived VEGFR2^{+} cells correlate significantly with VEGFR2^{+} cells in actual embryos.

In addition to VEGFR2^{+} cells, another receptor type of tyrosine kinase, platelet derived growth factor receptor α (PDGFRα), has been used to monitor the differentiation pathways in ES cell development (Kataoka et al., 1997; Nishikawa et al., 1998). Though PDGFRα is involved in the development of multiple cell lineages and begins to regularly appear from an early stage of embryogenesis (Soriano, 1997), its expression at 7.5 dpc and 8.5 dpc is mainly observed in two lineages; one is in mesodermal cells including paraxial mesoderm and somites, the other is in neural crest cells (NCC) and cranial mesenchymal cells (Takakura et al., 1997). Nascent mesodermal cells, mesenchymal cells and NCC begin to express PDGFRα upon transition from epithelial structures such as epiblasts and neuroepithelial cells (Schatteman et al., 1992). The phenotype of the PDGFRα-null mutant also suggested a common role for this receptor in development of mesodermal, mesenchymal and NCC lineages (Soriano, 1997; Tallquist and Soriano, 2003), implying that a common molecular mechanism underlies the generation of these lineages and that a part of this mechanism is also involved in expression of PDGFRα.

In our previous study, we analyzed the expression of PDGFRα and VEGFR2 in ES cell differentiation culture and defined four subpopulations, PDGFRα[+]VEGFR2^{+}, PDGFRα[−] VEGFR2^{+}, PDGFRα[+]VEGFR2^{−} and PDGFRα[−]VEGFR2^{−} (Nishikawa et al., 1998). While VEGFR2^{+} cells in this culture correspond to lateral mesodermal cells in the actual embryo, we and others showed PDGFRα[+]VEGFR2^{−} population includes paraxial mesoderm that can give rise to bone, cartilage and muscle cells (Nakayama et al., 2003; Sakurai et al., in press). The process by which ES cells differentiate to PDGFRα^{+} cells may represent, at least to some extent, a common process required for generation of PDGFRα^{+} cells from epithelial structures. One advantage of this experimental system is that PDGFRα can be used as a marker both for searching genes associated with this process and for purifying a sufficient number of PDGFRα^{+} cells for analyses.

We have been developing and establishing methods for selectively inducing ES cells to specific cell lineages corresponding to the three germ layers in actual embryos. To facilitate this process, gene expression profiles from ES-cell-derived cell populations were routinely created using Affyme-

trix oligonucleotide arrays. The expression profiles of the DNA microarray were stored and accumulated for use as a database, allowing the entire data set to be easily queried. By searching for genes showing a similar expression pattern to PDGFRα, the database was used to find genes regulating paraxial mesoderm and/or mesenchymal differentiation. Our analyses identified and listed a group of genes known to be important in differentiation of paraxial mesoderm, NCC and/or cranial mesenchymal cells. In addition to these extensively studied molecules, we also identified several molecules whose role in embryogenesis remains unknown.

In order to confirm the validity of our approach to discover novel genes, we chose the murine AT-rich interacting domain protein 3b (mARID3b) gene from this list of genes and characterized it in detail during in vivo embryogenesis. At 9.5 dpc, this molecule was expressed in both cranial mesenchyme and caudal mesoderm where PDGFRα expression overlaps (Takakura et al., 1997; Weston et al., 2004). Cardiovascular defects in mARID3b-null mice ensure embryonic lethality before 11.5 dpc, and the generation of cranial–mesenchymal cells in the first and second branchial arches (BA1 and BA2) was also found to be severely impaired. In mutant mice, mARID3b-expressing mesenchymal cells differentiated and migrated normally but failed to be maintained in BA1 and BA2. This study demonstrates that DNA microarray analysis of cells in ES cell differentiation culture is useful for identifying genes such as mARID3b, whose role in mouse embryogenesis has not yet been well characterized.

Materials and methods

ES cell culture and in vitro ES cell differentiation

CCE ES cells were maintained as described previously (Era and Witte, 2000). For gene targeting, TT2 ES cell lines were maintained as described previously (Yagi et al., 1993).

Induction of ES cell differentiation was performed as described previously (Nishikawa et al., 1998). CCE ES cells were seeded into 10-cm dishes coated with type IV collagen (BioCoat; Becton Dickinson Labware) at a density of 10^5 cells per dish in conditions of αMEM supplemented with 10% FCS and 50 μM 2-mercaptoethanol.

Antibodies and cell staining for FACS analysis and sorting

Rat MoAbs, APA5 (anti-PDGFRα) and AVAS12 (anti-VEGFR2) were prepared as described previously (Kataoka et al., 1997; Takakura et al., 1996). APA5 and AVAS12 were conjugated with biotin and allophycocyanin, respectively. Phycoerythrin-conjugated streptavidin (Pharmingen) was used to detect biotinylated-APA5 antibodies. For FACS analysis and sorting, day-4-differentiated ES cells were harvested and stained with these antibodies as described previously (Nishikawa et al., 1998).

Hybridization of cRNA to the oligonucleotide arrays

See Supplementary Fig. 6 information.

Bioinformatics analyses

Expression data from a number of samples were stored and analyzed using the eXintegrator system (http://www.cdb.riken.jp/scb/documentation/index.html).

The Affymetrix raw data set was transformed into Excel files by MicroSuite software (Affymetrix). The raw data in the Excel files were further analyzed using bioinformatics tools, NetAffix (Affymetrix) or an original Data analysis software, (Patent No. 2003-294553[1]). Genes were represented on Affymetrix arrays by sets of probes (known as probe sets) containing a number of paired probes, with each probe containing a background control. Comparisons in this analysis were carried out using individual probe pair profiles (foreground–background) rather than profiles of aggregate values for individual probe sets. Data from individual arrays were normalized by the median of the probe intensities on those chips before further analysis. Individual probe pair profiles were then normalized across the set of samples in the database by subtracting the mean and dividing by the standard deviation. Expression similarity values for pairs of probe sets were taken as the mean value of a set of all-against-all probe pair profile Euclidean distances (i.e. for two probe sets with 16 probes each, a total of 256 Euclidean distances were calculated and the mean of those distances taken). This calculation provides not only a measure of the similarity of the aggregate expression profile but also of the quality of the underlying data (as evidenced by co-variation of individual probe pair profiles).

Gene targeting

The 5′ and 3′ arms of the targeting construct were amplified from phage clones carrying mARID3b genomic genes by PCR method. Primers were: GCATCTTTAGCCTGCTCTGTTCTGC (forward) and GCTGCAGAGGCTC-CATTACTGTCT (reverse) for the 5′ genomic arm, and TAAGCAGGT-CAGTCTTTCTGCTG (forward) and AAGCCATGTTTAAGGGCTGG (reverse) for the 3′ genomic arm. The exon containing the ATG start codon was completely replaced by an internal ribosomal entry site (IRES)-β-galactosidase (LacZ) and PGK-Neo cDNAs flanked by loxP sites followed. After transfection, G418-resistant 150 colonies were selected and 8 correctly targeted clones obtained by Southern blot analysis. The probe was also amplified by PCR (forward—TTAAGCAGGTCAGTCTTTCT reverse—TCTAGAAACTAATTAGAACC). After transient expression of a Cre recombinase vector (Araki et al., 1997), the removal of the PGK-Neo cassette was confirmed by both sensitivity to G418 and Southern blot analysis. Two lines of chimeric mice were generated from two independent mARID3b+/− ES cell lines.

Breeding and genotyping of mice and embryos

Backcross mating to the C57BL/6 strain was performed more than five times. Tail tips or yolk sacs were used for genotyping by Southern blot analysis.

Northern blot analysis

mARID3b probe was amplified by PCR (primers: forward—ACAA-GACTCCCTTCTGATCCTCA and reverse—ATGGAGCCCTGGA-TAAGGTCTA) using cDNA of day-4-differentiated ES cells and labeled with αP^{32}-dCTP by Megaprime DNA labeling System (Amersham). Commercially available membranes–MTN™ (Multi Tissue Northern blot) 1, 2 (BD)–were used, and hybridization was performed according to the manufacturer's instructions. Membranes were re-hybridized with the probe for β-actin.

Whole-mount and section samples in situ hybridization

In situ hybridization was performed as described in the Anderson laboratory protocols (http://www.rodentia.com/wmc/docs/Big_In_Situ.html). Embryos were fixed in 4% paraformaldehyde overnight, and cryosections were used for section ISH. Anti-sense RNA probes were prepared from the probe construct in Northern blot analysis and labeled by DIG Labeling Kit (Roche) in accordance with the manufacturer's instructions. We used sense RNA probes as negative controls.

---

[1] An Open source client-server system for the analysis of Affymetrix microarray data. L.M. Jakt, M. Okada, S. Nishikawa (Genome Informatics Series (ISSN 0919-9454) No. 14, pp. 276–277, GIW 2003).

Histological analysis

For histological analysis, embryos were fixed in 4% paraformaldehyde overnight and embedded in paraffin wax for sectioning. Generally, 4-μm sections were cut and stained with Hematoxylin–Eosin or DAPI.

Terminal transferase-mediated dUTP-biotin nick end-labeling (TUNEL) assay was performed by ApoAlert DNA Fragmentation Assay Kit (BD). Apoptotic nuclei were visualized by green fluorescence and detected by confocal microscopy according to the instruction manual.

For LacZ staining, Embryos were fixed by 2% formaldehyde; 0.2% glutaraldehyde; 0.02% Nonidet P-40; 0.2 mM $MgCl_2$/phosphate-buffered saline (PBS) for 20 h and washed with 0.2 mM $MgCl_2$; 0.02% Nonident P-40/PBS and stained overnight with X-gal stain. Endothelial cell staining of whole-mount embryos and yolk sacs were performed using CD31 (PECAM1) antibody (Pharmingen) as described previously (Yamashita et al., 2000). Whole-mount immunohistostaining of PDGFRα antibody (antibody name: APA5) was performed according to the protocol described in previous report (Takakura et al., 1997).

Results

Identification of genes whose expression pattern is similar to that of PDGFRα

The expression of PDGFRα is mainly observed in cranial mesenchyme, paraxial mesoderm and somites during early mouse embryogenesis (Supplementary Fig. 1) (Takakura et al., 1997; Zhang et al., 1998). Our previous studies showed that this particular gene could be used to monitor the differentiation of paraxial mesoderm and mesenchymal cells during in vitro ES cell differentiation (Fig. 1A) (Kataoka et al., 1997; Nishikawa et al., 1998). Our recent experiments demonstrated that PDGFRα$^+$VEGFR2$^+$ progenitors could give rise to both PDGFRα$^+$VEGFR2$^-$ and PDGFRα$^-$VEGFR2$^+$ populations, the former has a potential to give rise to the mesenchymal cell lineage while the latter corresponds to lateral mesoderm (Figs. 1A and B) (Sakurai et al., in press). This putative model for ES cell differentiation to PDGFRα$^+$ cells implies that this process could be used as a model for the transition of epithelial cells to PDGFRα$^+$ mesenchymal cells.

We have accumulated data of DNA microarray analysis of various intermediates in ES cell differentiation culture and defined them in terms of differentiation markers that are utilized for cell sorting by FACS. In addition to the three populations described above, this database contained VE-cadherin$^+$ cells, undifferentiated ES cells, aortic endothelial cells and VEGFR2$^+$ cells that were not fractionated further, thus including both PDGFRα$^+$ and PDGFRα$^-$ populations.

To isolate the candidate genes, gene expression patterns were simply compared with those of PDGFRα. Affymetrix probe sets were sorted by similarity of expression to a probe set representing PDGFRα using a modified Euclidean distance measurement (Fig. 1C, and see Materials and methods). This method of data mining was expected to identify genes that exhibit similar expression patterns to PDGFRα in vivo. Table 1 and Supplementary Fig. 2 list the 30 genes with expression patterns of highest similarity to PDGFRα. To date, 24 out of the 30 genes in the list have
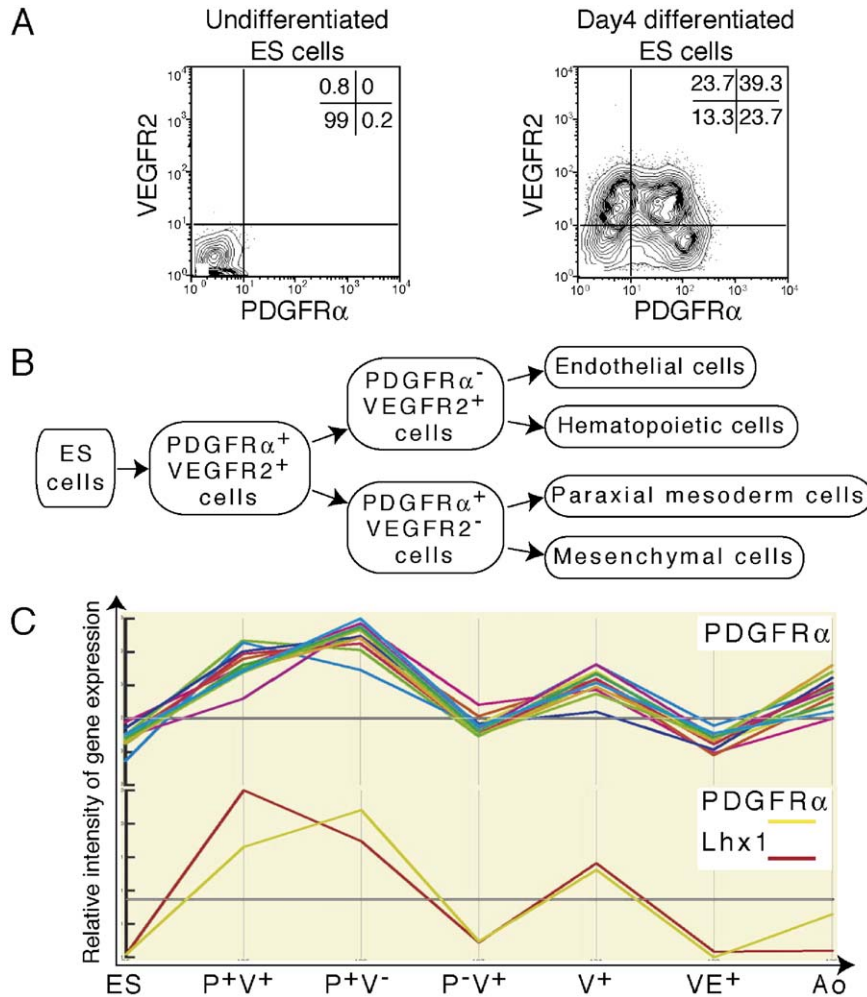
Fig. 1. DNA microarray analyses of ES-cell-derived PDGFRα[+] populations. (A) Expression patterns of PDGFRα and VEGFR2 during in vitro ES cell differentiation. Undifferentiated ES cells do not express either receptor (left panel), whereas day-4-differentiated ES cells do (right panel). On day 4, differentiated ES cells expressing both markers are classified into three populations, PDGFRα[+]VEGFR2^{+}, PDGFRα[+]VEGFR2^{−} and PDGFRα[−]VEGFR2^{+}. (B) A model for differentiation from ES cells to PDGFRα[+] and VEGFR2^{+} cell lineages. Our previous analysis revealed three types of cell population in day-4-differentiated ES cells. The PDGFRα[+]VEGFR2^{+} population can give rise to both PDGFRα[−]VEGFR2^{+} and PDGFRα[+]VEGFR2^{−} populations. PDGFRα[−]VEGFR2^{+} cells eventually differentiate into endothelial and hematopoietic cells. However, our data indicated that PDGFRα[+]VEGFR2^{−} cells display very similar differentiation potential to paraxial mesoderm and mesenchymal cells in actual mouse embryos (Sakurai et al., in press). (C) Procedure to select genes showing similar expression patterns to that of PDGFRα. Microarray data of seven distinct populations, undifferentiated ES cells (ES), PDGFRα[+]VEGFR2^{+} cells (P[+]V[+]), PDGFRα[+]VEGFR2^{−} cells (P[+]V[−]), PDGFRα[+]VEGFR2^{+} cells (P[−]V[+]), VEGFR2^{+} cells (V[+]) that contain both PDGFRα[+] and PDGFRα^{−} cells, VE-cadherin [+] cells (VE[+]) and aortic endothelial cells (Ao) were selected from our database. The upper panel shows relative expression level of PDGFRα in each population. Each value connected by the lines represents data of different oligo-probes for PDGFRα gene, which are normalized so as to reduce the variation among probes (see Materials and methods). To simplify analyses, mean values of expression intensities are also measured and blotted (lower panel and Supplementary Fig. 2). Genes that showed a similar expression pattern to PDGFRα (yellow line) were selected by our software as described in Materials and methods. Lhx1 (red line) is the gene ranked as the closest match. The patterns of the top 30 genes are presented in Supplementary Fig. 2.

been characterized in terms of their embryonic expression, and phenotype analyses of gene knock out mice have been reported for 22 of them (references in Supplementary Fig. 3). Eighteen genes are expressed in mesodermal and mesenchymal cells, and, more specifically, thirteen of them show more restricted expression patterns in either paraxial mesoderm or cranial mesenchyme (indicated by a star in Table 1). Seven of the genes, #7 (Mesp1), #9 (Lfng), #20 (Gsc), #22 (Cyp26), #23 (Msx2), #28 (Msx1) and #30 (Pitx2), were shown to be embryonic lethal by null mutation due to obvious defects in the differentiation of paraxial mesoderm or cranial mesenchymal cells (Supplementary Fig.

3). Among transcriptional factors in the list, null mutant mice of gene encoding #1 (Lhx1), #4 (Eomes), #10 (Sna), #18 (Six2), #24 (Sox4) and #29 (Lef1) have been reported to display defects in development of either mesodermal, mesenchymal or both. This list contains also cadherins, such as #15 (Cdh11) and #26 (Cdh2), whose roles were implicated in the migration of NCC during the epithelial–mesenchymal transition. #3 (Sfp3), #14 (Smad1) and #16 (Rbp1) are signaling molecules that are known to be involved in Wnt, BMP and retinoic acid, respectively, which are crucial in the development of many cell lineage including mesoderm and mesenchyme.

Table 1
List of the top 30 genes showing highest similarity of expression patterns to PDGFRα expression

	Gene symbol	Gene name	Affymetrix ID	GeneBank ID number	Expression (7.5dpc–9.5dpc)	
1	**Lhx1**	LIM homeobox protein 1	92961_at	NM_008498	Primitive streak, notochord, node, lateral plate mesenchyme, mesoderm	
2	**Slit3**	Slit homologe 3	112022_at	AF_144629	Midline of the neural groove, the commissural plate otic vesicle, clefts between 1st and 2nd arches	
3	**Sfrp3***	Secreted frizzled-related sequence protein 3	104672_at	NM_011356	Trunk mesenchyme, paraxial mesenchyme	
4	**Eomes**	Eomesodermin homolog (Xenopus laevis)	103532_at	NM_010136	Primitive streak, extraembryonic component	
5	**Evx1**	Even skipped homeotic gene 1 homolog	98815_at	NM_007966	Primitive streak, tail, parienta endoderm	
6	**Gas1**	Growth arrest specific 1	94813_at	NM_008086	Primitive streak, somite, surface ectoderm, lateral plate mesoderm, splanchnic mesoderm,	
7	**Mesp1***	Mesoderm posterior 1	102795_at	NM_008588	Mesoderm, allantois, mesenchyme	
8	**Unkown**	EST 89698 (unigene) Rho GTPase activating protein 7 (predict)	112699_at	NM_015802	**Not reported**	
9	**Lfng***	Lunatic fringe gene homologe	114102_at	NM_008494	Node, pro-rhombomere, rhombomere03,05, paraxial mesenchyme, unsegmented mesenchyme	
10	**Sna***	Snail homolog 1 (Drosophila)	103830_at	NM_011427	Primitive streak, pariental endoderm, 1st 2nd arch mesenchyme derived	
11	**ARID3b**	AT rich interactive domain 3B (Bright like)	103970_at	NM_019689	**Not reported**	
12	**Pbx3**	pre B-cell leukemia transcription factor 3	93615_at	NM_016768	Central nerve system	
13	**Myl7**	Myosin, light polypeptide 7, regulatory	100403_at	NM_022879	Heart, cardiac muscle,	
14	**Smad1**	MAD homolog 1 (Drosophila)	102983_at	NM_008539	Primitive streak, mesoderm	
15	**cdh11***	Cadherin 11	100006_at	NM_009866	Periopic mesencyme	
16	**Rbp1***	Retinol binding protein 1	104716_at	NM_011254	Primitive streak, rhombomere 1–7, branchial arch, paraxial mesenchyme, trunk mesenchyme, tail bud	
17	**car14**	Carbonic anhydrase 14	161434_r_at	NM_011797	**Not reported**	
18	**six2***	Sine oculis-related homeobox 2 homolog	98839_at	NM_011380	Head mesenchyme, 1st and 2nd arch,	
19	**Efna3**	Ephrin A3	100289_at	XM_204001	**Not reported**	
20	**Gsc***	Goosecoid	94187_at	NM_010351	Node, Primitive streak, 1st arch	
21	**Unknown**	Hypothetial protein FLJ22116 (predict)	100887_at		**Not reported**	
22	**Cyp26***	Cytochrome P450 family 26	98320_at	NM_007811	Head mesenchyme, 1st and 2nd arch	
23	**Msx2***	Homeo box, msh-like 2	102956_at	NM_013601	1st and 2nd arch, mesencyme dereived from neural crest	
24	**sox4**	SRY-box containing gene 4	101430_at	NM_009238	Head process, most posterior end of the neural tube	
25	**Rab34**	RAB34, member of RAS oncogene family	160317_at	NM_033475	**Not reported**	
26	**cdh2***	N-cadherin	102852_at	NM_007664	Paraxial mesenchyme, somite, notochord	
27	**Plxna2**	PlexinA2	106447_at	NM_008883	Central nervous system	
28	**Msx1***	Homeo box, msh-like 1	111927_at	NM_010835	Spinal cord, midbrain, head messenchyme, branchhial arch, limb bud	
29	**Lef1**	Lymphoid enhancer binding factor 1	103628_at	NM_010703	Primitive streak, diencephalon, telecephalon	
30	**Pitx2***	Paired-like homeodomain transcription factor 2	102788_s_at	NM_011098	Head mesenchyme, lateral plate mesencyme, 1st arch	

Expression sites of each listed gene in 7.5–9.5 dpc embryos are described and represented by color marks as indicated in the table. Eighteen out of 30 genes in this list are expressed either in mesodermal or mesenchymal cells. Five of them, #1, #3, #9, #15 and #26, are expressed in both. While most of them have been characterized to some extent, data concerning the functions of #8, #11, #21 and #25 in embryogenesis are not available to date. Asterisk marks 13 of 30 genes which exhibit the restricted expression in either paraxial mesoderm or cranial mesenchyme.

Expression: ■ mesoderm, ■ mesoderm (paraxial), ■ mesenchyme, ■ mesenchyme (Branchial archs).

While it is difficult to formally rule out the possibility that those genes are listed by a simple coincidence, we believe that many of genes in this list are indeed known to be involved in development of mesodermal/mesenchymal cells as we have expected. Hence, our approach using DNA microarray analysis in ES cell differentiation culture is useful for mining genes that play an indispensable role in a particular process of mouse embryogenesis.

ARID3b gene

As the functions and expression patterns of the four molecules in this list, #8 (unknown), #11 (mARID3b), #21 (unknown) and #25 (Rab34) remain uncharacterized, their expression patterns in early mouse embryo were initially assessed by whole-mount in situ hybridization (ISH). While we succeeded to obtain specific staining by using probe of #11 (mARID3b), further experiments are still needed for determine expression pattern of other three genes. In addition, the complete cDNA sequences of mARID3b were available in the NCBI database, though its role in embryogenesis remains uncharacterized. Hence, we decided to focus on mARID3b in this study.

ARID3 is divided into two molecules, 3a and 3b, which are encoded by distinct genes (Kortschak et al., 2000). The deduced amino acid sequence of mARID3b (568a.a) is very similar to human ARID3B (hARID3B) (560a.a.) (85% homology of amino acids). Though the overall similarity between mARID3b and hARID3a is not so high (39.6%), a high degree of similarity among DNA binding domains is

conserved among ARID3 molecules (84%) (Supplementary Fig. 4).

ARID3B was originally discovered as a protein binding to Rb1 (Numata et al., 1999), one of the major cell cycle regulators (Weinberg, 1991), and itself a member of the ARID family with an ARID motif that can bind to an AT-rich DNA sequence (Iwahara et al., 2002). The ARID family members are conserved from yeast to human and have been shown to be involved in a number of processes including cell cycle regulation, senescence bypass, transcriptional regulation and chromatin regulation (Kortschak et al., 2000; Wilsker et al., 2002). In particular, Dri, the homologue of ARID3 in *Drosophila*, plays an essential role in early embryogenesis (Shandala et al., 1999). The similarity of expression patterns between PDGFRα and mARID3b, as well as the function of the ARID family molecules during embryogenesis, led us to characterize mARID3b in detail to determine its role in the differentiation of paraxial mesoderm and mesenchymal cells.

ARID3b expression

In addition to the similarity of the predicted protein sequences, the expression pattern of mARID3b in adult tissues is very similar to that of hARID3b (Numata et al., 1999). A single 4.2 kbp mRNA with the highest signal was detected in testes by Northern blot analysis, while weaker expression was also detected in prostate, thyroid and thymus. No signal was detected in other organs, including liver, spleen, heart, brain, lung, muscle and kidney (Fig. 2A).

mARID3b expression during early embryogenesis was then analyzed using a whole-mount ISH technique. It is first detected in 7.0–7.5 dpc embryos at the boundary of the primitive streak and paraxial mesoderm and also at the
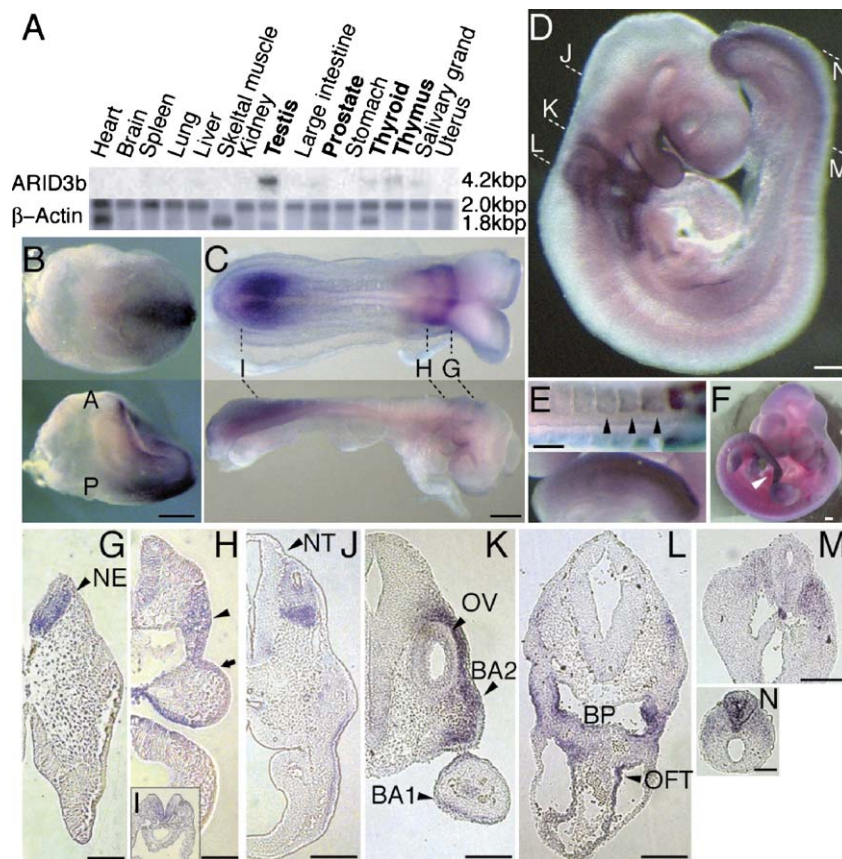

Fig. 2. Expression of mARID3b in mouse adult tissues and embryo. (A) Northern blot analysis of mARID3b gene in mouse adult tissues. The strongest signal (4.2 kbp) is detected in testes. A weak signal is observed in prostate, thyroid and thymus (upper panel). β-actin probe was used as a positive control (lower panel). (B–N) mARID3b expression in mouse embryo. Whole-mount in site hybridization (ISH) (B–F). In 7.5 dpc embryo, mARID3b is expressed at the boundary of the primitive streak, paraxial mesoderm and in the junction between neural and surface ectoderm (B, upper: anterior view and lower: lateral view). In 8.5 dpc embryo, it is expressed in the neural plate, prorhombomere, tail bud and precaudal somites (C, upper: anterior view and lower: lateral view). In 9.5 dpc embryo (D and E), expression is observed in the distal region of BA1 (D), from the proximal to the distal region of the BA2 (D), precaudal somites (upper panel in E, indicated by arrowheads), pre-somitic mesoderm (lower panel in E) and the distal end of the neural tube (lower panel in E). In 10.5 dpc, this expression disappears except for the tail tip (F, indicated by arrowhead). ISH of sections. (G–N) Sectioned levels are indicated in panels C and D. In 8.5 dpc embryo (G–I), mARID3b is expressed in the neuroepithelium of the prorhombomere (G), dorsal part of the first branchial groove that contains the prospective BA2 (H, arrowhead) and the ectoderm in BA1 (H, arrow). Its expression is also observed in caudal neuroepithelium (I). In 9.5 dpc embryo (J–N), mARID3b is expressed in the facio-acoustic neural crest complex (J), mesenchymal tissues in the lateral portion of OV (K), BA2 and the surface of BA1 (K), a pharyngeal ectoderm of 2nd BP (L), a wall of outflow tract (L), pre-somitic mesoderm and mesenchyme at the caudal region (M) and the neural tube at the caudal end (N). Abbreviations: (A) anterior; (P) posterior; (NE) neuroepithelium; (BA) branchial arch; (NT) neural tube; (OV) optic vesicle; (BP) branchial pouch; (OFT) outflow tract. Scale bars: 200 μm (B–F, J–M); 100 μm (G, H, N).

junction between the neural and surface ectoderms (Fig. 2B). In 8.5 dpc embryos, it is expressed in the prorhombomere and the tail bud, where the neural tube remains open (Fig. 2C), although expression was barely detectable in the trunk area where the neural tube is already closed. The signal was also detected in a few nascent somites. In 9.5 dpc embryos, a high level of expression is detected from the proximal to the distal regions of the BA2 and BA3 (Fig. 2D). In the BA1, the expression was more restricted to the distal region, and expression continues in the tail bud and nascent somites (Fig. 2E). At 10.5 dpc, mARID3b expression was observed to be down-regulated in the regions of BAs and somites, whereas it was still maintained in the tail tip (Fig. 2F).

On transverse sections of 8.5 dpc embryos, the expression was observed in neuroepithelium overlying origin of trigeminal neural crest (Fig. 2G), a dorsal side of tissue at first branchial groove (Fig. 2H), which contains a prospective BA2 tissue, and an epithelium of BA1 (Fig. 2H). The expression was also detected in a caudal neuroepithelium and mesoderm (Fig. 2I). At 9.5 dpc, a high level of mARID3b expression was detected mostly in mesenchymal cells in the facio-acoustic neural crest complex (Fig. 2J), in the lateral portion of the otic vesicle (Fig. 2K), in the mesenchyme of BA2 (Fig. 2K) and in the caudal region. Expression was also observed in the ectoderm of BA1 (Fig. 2K), the pharyngeal ectoderm of the 1st branchial pouch and the wall of the outflow tract (OFT) (Fig. 2L). In the caudal region, expression was detected in some newly formed somites and neural tubes (Figs. 2M and N).

Our analyses of mARID3b expression showed that (1) mARID3b is strongly expressed in cranial mesenchyme and caudal mesoderm; (2) the expression of cranial mesenchyme is rapidly down-regulated by 10.5 dpc; (3) in adult tissue, a few organs, including testes, prostate, thyroid and thymus, express this gene. Of particular note is that a significant overlap exists between the mARID3b$^+$ and PDGFRα^+ areas in mesodermal and cranial mesenchymal tissues, except in the somite region. In 8.5 dpc and 9.5 dpc, PDGFRα is widely expressed in almost all somites (Takakura et al., 1997) (Supplementary Fig. 1), whereas mARID3b is expressed restrictively in newly formed somites.

mARID3b-null phenotype

To analyze the embryonic function of mARID3b, we generated mARID3b-null mice according to the knockout strategy described in Figs. 3A and B. This procedure results in an allele whose expression can be tracked by LacZ expression.

Sibling matings of heterozygotes produced no live born homozygous pups (data not shown), indicating lethality in the mutant embryos. Timed pregnant mothers were dissected on embryonic days 7.5 dpc to 15.5 dpc to establish the number and genotypes of the fetus in each litter (Fig. 3C). As the number of homozygous embryos dropped abruptly at 12.5 dpc, we concentrated our analysis on embryos younger than 12.5 days.

At 9.5 dpc, approximately 60% of null embryos showed dilated hearts, head deformities and small BAs (left panel in Fig. 4A). The remaining 40% of the null embryos displayed only

small body size (center panel in Fig. 4A). The phenotype of 10.5 dpc-null embryo was even more severe than that of 9.5 dpc. Null embryos displayed two distinct phenotypes; one group showed only growth retardation (40%, 6/15) (center embryo in Fig. 4B), while the other group, in addition to growth retardation, had an arrested heart looping with dilated pericardial sacs, wavy neural tube (lower left panel in Fig. 4B), hypoplasia of BAs and a small craniofacial structure (60%, 9/15) (left embryo in Fig. 4B). Null mutants rarely survived to 12.5 dpc (4.7%, 2/43). In these surviving mutants, the major phenotypes have (1) massive bleeding around major vessels, heart and liver (Supplementary Fig. 5A), (2) wavy neural tube (Supplementary Fig. 5B) and (3) small BAs (Supplementary Fig. 5C).

Defect in vascular remodeling

The 10.5 dpc-null mutants were classified into two groups: embryos with growth retardation without obvious malformations and those with severe malformations. The null mutant mice with severe phenotypes exhibited abnormalities in their cardiovascular system (Figs. 4C–F). At 10.5 dpc, although hematopoietic cells were detected in blood vessels, any distinction between large and small blood vessels was barely observable in the yolk sac of mARID3b-null mice (Supplementary Fig. 5D). To further examine this defect, we examined the expression of CD31 (PECAM1), an endothelial cell marker. Though CD31$^+$ endothelial cells differentiate to form a vascular network in the yolk sacs of the null mutants, vascular remodeling from the primitive plexus to the higher order
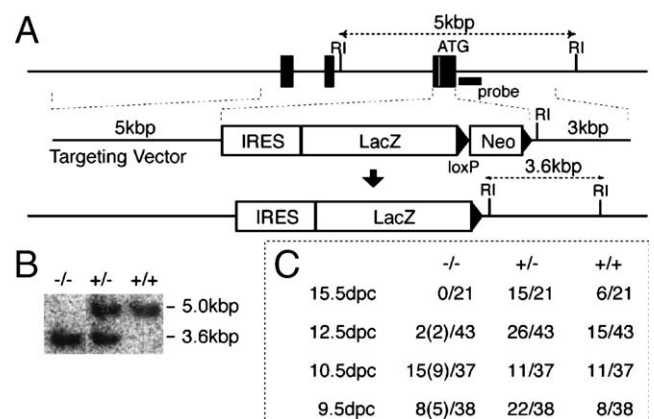

Fig. 3. Generation of mARID3b-null mouse. (A) Strategy for producing mARID3b-null mouse. The exon, including the starting codon, is replaced by an internal ribosomal entry site (IRES) and a LacZ cassette. Endogenous mARID3b expression can be tracked by the expression of LacZ. The PGK-neo cassette (Neo) is flanked by loxP sites (triangles) for subsequent removal by cre-recombinase. The flanking genomic probes used for Southern blot hybridization are highlighted by thick lines. RI: *Eco*RI. (B) Southern blot analysis of 10.5 dpc embryo. Genomic DNA obtained from yolk sacs was digested with *Eco*RI and hybridized with the probe shown in panel A. Fragments obtained from wild type and targeted alleles are indicated. (C) Embryonic lethality of mARID3b-null mouse. Frequencies of genotype obtained from intercrosses of mARID3b+/−. No mARID3b-null embryo was obtained after 15.5 dpc. Though some null embryos survived until 12.5 dpc, almost all died before 11.5 dpc. Numbers in parenthesis represent number of embryos showing typical phenotype.
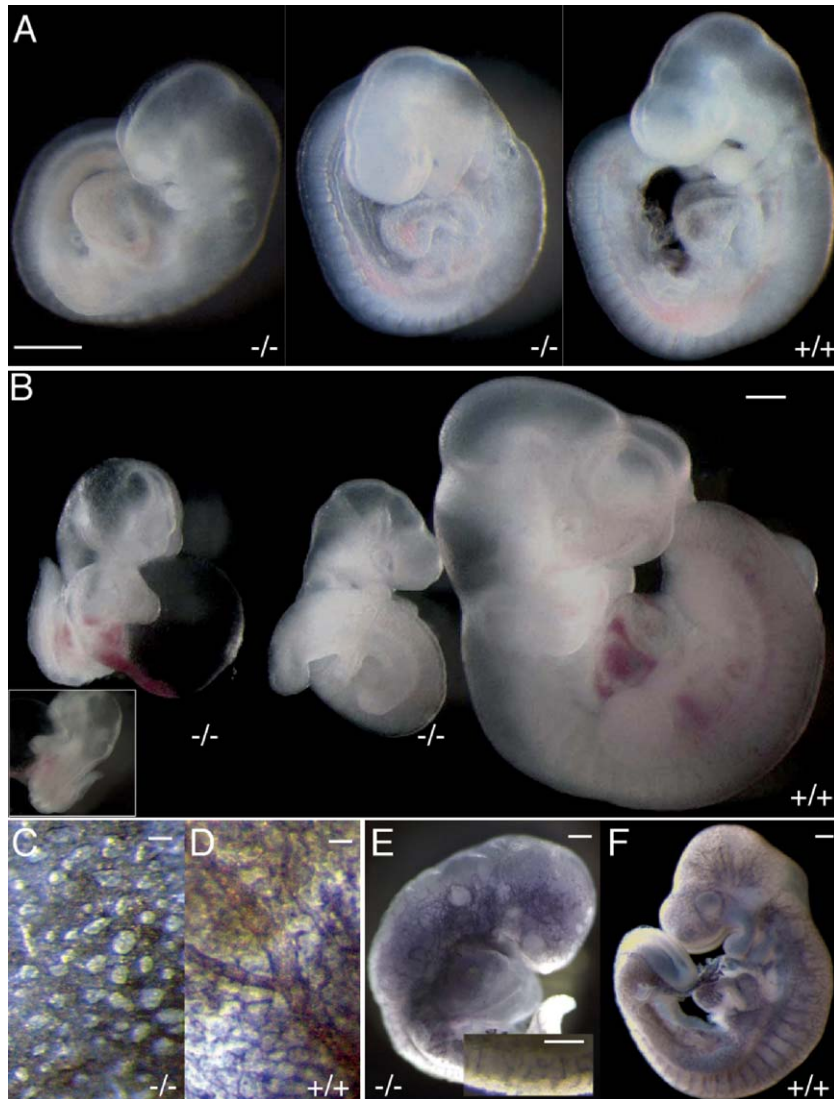
Fig. 4. Phenotype of mARID3b-null embryo. (A and B) Phenotype of mARID3b-null embryos at 9.5 dpc (A) and 10.5 dpc (B). At 9.5 dpc, approximately 60% of total null embryos display a dilated heart and small BA1 (left embryo in A). The remaining 40% show only growth retardation (middle embryo in A), compared to wild type embryos (right embryo in A). At 10.5 dpc, approximately 60% of null embryos (left embryo in B) exhibit arrested heart tube looping, dilated pericardial sacs, hypoplasia of BAs, small craniofacial structures and wavy neural tubes (left lower small panel in B), whereas the remainders show growth retardation (middle embryo in B), compared with wild type littermates (right embryo in B). Scale bars indicate 500 μm. (C–F) Defect of vascular remodeling in mARID3b-null embryos. Endothelial cells are visualized by immunostaining of CD31 (PECAM1). The vasculature in the yolk sac of the mutant (C) and the control (D) mice. A distinction between large and small vessels is found only in the control yolk sac. The vasculature in the embryo of the null mutant (E) and control (F) mouse. In the mutant embryo, vascular remodeling is severely impaired. Despite the severe defect in remodeling, intersomitic arteries develop from the dorsal aorta of the null mutant (inset picture in E). Scale bars: 100 μm (C and D); 200 μm (E and F).

architecture and retaining distinction between large and small blood vessels is severely impaired, compared to the yolk sac of the wild type embryo (Figs. 4C and D). Vascular remodeling is severely impaired in actual mutant embryos (Figs. 4E and F), though dorsal aorta and intersomitic arteries are formed to a certain extent (inset in Fig. 4E). This suggests that vascular endothelial cells are generated in the null mutant and form the primitive plexus but fail to undergo remodeling. Despite such a severe phenotype in the vascular system, mARID3b expression was barely detectable in both vascular endothelial cells and mural cells of wild type embryos (Fig. 2D). To confirm the absence of mARID3b expression in endothelial cells, we purified $CD31^+CD45^-$ fractions from dissociated 9.5 dpc

embryos and analyzed mARID3b expression by RT-PCR. No mARID3b expression was detected in this population (Supplementary Figs. 5E and F).

In severe phenotype mutants at 10.5 dpc, heart formation was arrested in the middle of the looping of the heart tube (Fig. 4B). Despite this, cardiac muscles were present (Supplementary Figs. 5G and H), and beating was indeed detected at 9.5 dpc. Moreover, the expression of mARID3b is barely observed in the developing heart muscle (Figs. 2D and L, Supplementary Figs. 5I and J). Taken together, mARID3b may not have a cell-autonomous role in the differentiation of endothelial cells and cardiac muscles.

Severe impairment in generation of cranial mesenchymal cell in the mARID3b-null mutant

The most conspicuous defects in 10.5 dpc-null mutants consisted of hypoplasia of BAs and small craniofacial structures. Histological analysis of sections revealed a marked reduction in the number of mesenchymal cells putatively derived from neural fold. In normal 9.5 dpc embryos, BA1 and BA2 contain dense populations of mesenchymal cells, while they are almost completely absent from the same regions in the mutant embryos (Figs. 5A and B). A similar reduction in cell number is also found in the facio-acoustic neural crest complex and in the vicinity of the otic vesicles (Figs. 5A and B). In contrast to the cranial region, the reduction of mesenchymal cells in the trunk of null mutants is less conspicuous, though their development is still impaired to some extent (data not shown).

In section analysis of the heart, clots, probably due to coagulation, are often found at the OFT of the heart in mutant embryos, suggesting the presence of a blockade in circulation (Figs. 5C and D). In keeping with this hypothesis, the dorsal aorta and the cardinal vein in the section at OFT level are often difficult to distinguish (Figs. 5C and D), whereas the dorsal aorta in the trunk was easily distinguishable from other vessels (lower small panel in Fig. 5C). As the OFT tissue is known to be derived from $PDGFR\alpha^+$ cranial mesenchymal cells which have an essential role in the proper formation of OFT (Tallquist and Soriano, 2003), the defect of OFT formation is consistent with the significant decrease in the number of cranial mesenchymal cells.

In order to investigate whether or not the loss of mesenchymal cells is ascribed to enhanced apoptosis, we performed TUNEL and DAPI staining. Extensive increase of TUNEL-stained cells was detected in both NCC complex and BA1 and 2 (Figs. 5E and
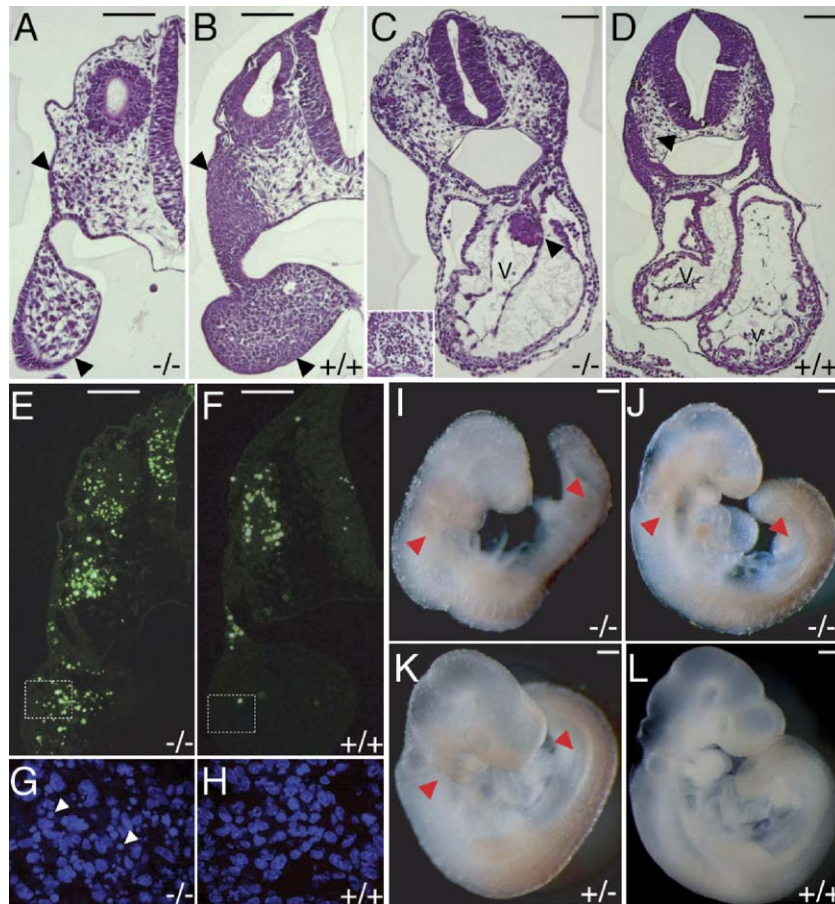

Fig. 5. Severe reduction of cranial mesenchymal cells in mARID3b-null embryo. (A–D) HE staining of sections at BA level (A and B) and OFT level (C and D). At 9.5 dpc, cellularity of mesenchyme tissue in BA1 and BA2 is severely reduced (arrowheads in A). In contrast, BA1 and BA2 contain dense populations of cranial–mesenchymal cells (arrowheads in B). At the OFT level, the density of cranial mesenchymal cells is markedly reduced, and the dorsal aorta and cardinal vein are barely detected (C), though the dorsal aorta can be easily recognized at the caudal level (inset in C). Cell aggregates, presumably due to coagulation, were detected at the OFT (C, indicated by an arrowhead), and their hemorrhaging into the pericardial cavity is frequently observed in null embryos (C). The dorsal aorta (arrowhead in D) and cardinal vein are easily detected in wild type embryo (D). Abbreviation: (V) ventricular chamber. (E and F) TUNEL analysis of cranial mesenchyme. TUNEL$^+$ cells are fluorescent indicating active apoptosis. Transverse section at the level of the BAs in 9.5 dpc mARID3b-null mutant (E) shows an extensive increase of apoptosis not only in the facial–acoustic neural crest complex but also in the mesenchyme of BA1 and 2, compared to the wild type embryo (F). This increase is also observed in the head neural tube (E). (G and H) 4′-6-Diamidino-2-phenylindole (DAPI) staining of serial sections to those shown in panels E and F, respectively. Highly magnified views of areas marked by squares in panels E and F are shown in panels G and H. In contrast to wild type embryos (H), many nuclear fragmentations are observed in mutant (G, indicated by arrowheads), suggesting that the cell death with apoptosis in cranial mesenchymal cells is enhanced in the null embryo. (I–L) LacZ tracking of mARID3b$^+$ cells. LacZ expression indicated by red arrowheads is detected at the distal end of BA1 and BA2, not only in the mutant embryo with a mild phenotype (I) but also in those with severe phenotype (J). The signal is detected in the heterozygous embryo (K) but not in the wild type embryo (L). Scale bars indicate 200 μm.

F). Unexpectedly, enhancement of apoptosis was also observed in head neural tube. Consistent with these results, an increase in the number of dead cells with fragmented nuclei was observed in regions that are normally filled with mARID3b-expressing cranial mesenchymal cells (Figs. 5G and H). This increase in apoptotic and dead cells, however, was not observed in the caudal region where mARID3b-expressing mesoderm cells exit (data not shown). Taken together, these results suggest that apoptosis is the major cellular mechanism underlying this defect of cranial mesenchymal cells.

In an attempt to further specify the cellular basis for the failure to generate cranial mesenchymal cells, we investigated the distribution of LacZ$^+$ cells in null mutant embryos, which represent an mARID3b$^+$ lineage but are generated in the absence of mARID3b function. LacZ staining was detected in the regions where endogenous mARID3b expression is observed, regardless of phenotypic severity (Figs. 5I–L). This shows that, although cells expressing mARID3b were generated and migrated into the distal region of BAs, they could not be maintained. These results also suggest a role for mARID3b in cranial mesenchymal cell survival.

Comparison with PDGFRα KO mouse

mARID3b KO embryos share a number of common features with PDGFRα KO embryos, such as wavy neural tubes, failure in cardiogenesis with an enlarged pericardium, facial deformity and poorly formed BAs, especially so when the mutant allele is introduced into a C57BL/6 background (Soriano, 1997) (Figs. 6A and B). Although mARID3b is expressed more transiently and in more restricted areas than PDGFRα, symptoms are actually more severe in mARID3b- than PDGFRα-null embryos. Despite this, mARID3b expression is detected in Ph/Ph mouse that have large deletions, including the gene encoding PDGFRα (Fig. 6C) (Stephenson et al., 1991). Likewise, PDGFRα$^+$ mesenchymal cells are present in mARID3b-null mouse (Fig. 6D). It is therefore likely that the two molecules are required for independent processes during differentiation of paraxial mesoderm and mesenchyme derived from neural fold.

Discussion

Combinatory use of ES cell cultures and microarray analysis for identifying genes involved in early embryogenesis

Microarray technology is well suited to comprehensive analyses of changes in transcriptional activity that underlie cell specification during embryogenesis (Debouck and Goodfellow, 1999; Smith and Greenfield, 2003). However, use of this technology for analyzing early mouse embryogenesis has so far remained limited due to difficulties in collecting a sufficient number of specific cell populations from developing embryos. Our group, as well as others, has shown that various intermediates appearing in the course of embryogenesis can be induced and purified from ES cell differentiation cultures (Kabrun et al., 1997; Nishikawa et al., 1998). While the cell
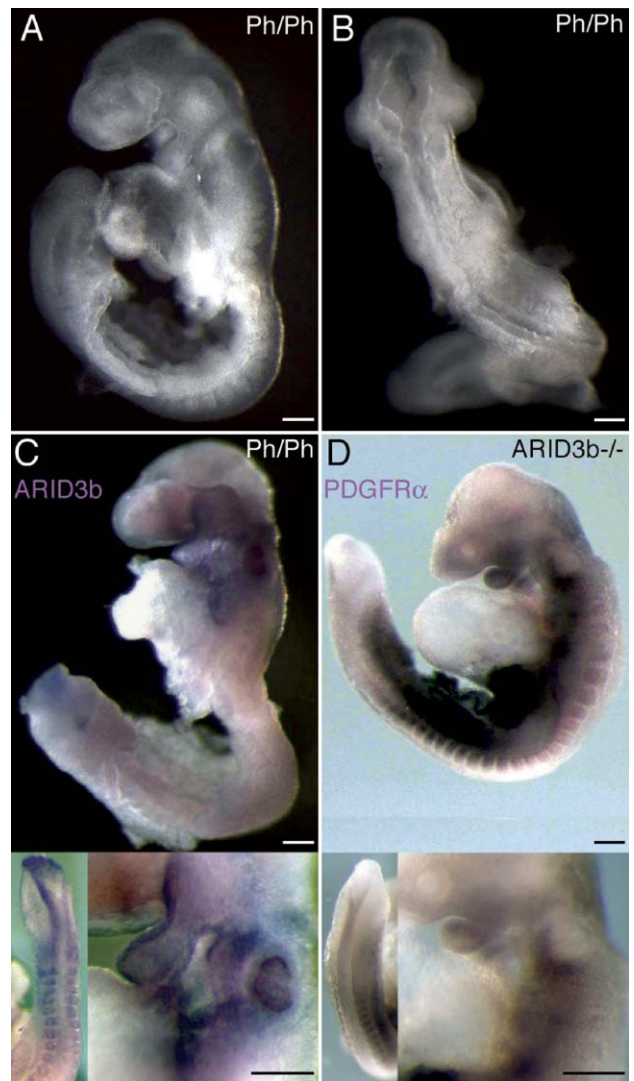

Fig. 6. Similarity between mARID3b-null and PDGFRα-null mutant mice. (A and B) Phenotype of Ph/Ph mutant mouse. At 9.5 dpc, the phenotype of the Ph/Ph mutant that bears a large deletion in the region containing whole PDGFRα coding region is similar to that of mARID3b-null mutants. Ph/Ph embryo shows poorly formed BAs, failure in cardiogenesis with an enlarged pericardium (A) and wavy neural tube (B). (C) mARID3b expression in 9.5 dpc Ph/Ph mutant mouse. By whole-mount ISH of mARID3b, mARID3b expression was detected in BAs (right lower panel in C) and the caudal region containing neural tube and somites (left lower panel in C). (D) PDGFRα expression in 9.5 dpc mARID3b-null mouse. The expression of PDGFRα is detected in BAs (right lower panel in D) and nascent somites (left lower panel in D). These results suggest that mARID3b and PDGFRα do not interact directly. Scale bars indicate 200 μm.

variety obtained by the currently available technology is limited, this situation will improve along with development of new technologies for cell culture and purification. As a result, ES cell culture will become of increasing importance as a non-substitutable cell source for DNA microarray analysis of embryonic processes.

However, we are also aware of problems inherent in this experimental system. Any given populations, even though purified by using multiple differentiation markers, are likely to contain heterogeneous populations as available markers are always limited, and the phenotypes of cells are continuously

changing even within a population defined by a set of particular markers. Microarray data of any given population may not represent a particular status but rather a general tendency of a differentiation course. We therefore believe that an important feature in using cells harvested from ES cell differentiation culture is to collect enough data in such a way as to reflect this general tendency. Keeping this concept in mind, we performed microarray analysis of cell populations whenever a particular cell population was obtained and stored all data in such a way that a number of different questions could be addressed.

In this study, PDGFRα was chosen as a key marker for mesodermal and mesenchymal differentiation, and several intermediates in the mesoderm differentiation pathways were analyzed. Using our own software, we listed 30 genes with expression patterns similar to PDGFRα. As we could list many genes that have been implicated in development of either mesoderm, cranial mesenchyme or NCC, our approach appears useful for identifying genes involved in embryonic development. However, it should be noted that 8 distinct samples analyzed in this study contain neither NCC nor cranial mesenchymal cells. Thus, our method for gene discovery, which compared multiple samples derived from ES cell differentiation cultures, does not necessarily list genes that are expressed specifically in the development of intermediates selected for analysis. Nonetheless, as PDGFRα is expressed also in cranial mesenchyme and NCC, our method may have an ability to rank genes commonly involved in multiple differentiation pathways for PDGFRα$^+$ cells, though underlying rationale of our application is yet to be determined by applying it to different settings.

Role of mARID3b in embryogenesis

In addition to molecules that have already been characterized to a significant extent, our list of 30 genes with expression patterns similar to PDGFRα includes several molecules whose role in embryogenesis has been yet to be explored. One such molecule, mARID3b, expressed mainly in paraxial mesoderm and cranial mesenchyme, was further analyzed in this study. We generated mARID3b-null mutant mice in which lacZ expression is used for tracking endogenous mARID3b expression.

The null mutants showed an embryonic lethality before 11.5 dpc. While the phenotypes of mutant embryos do vary among embryos, the three most common defects were: (1) wavy neural tube, (2) small branchial arches and (3) defect of cardiovascular system. It is interesting that these defects have also been found in PDGFRα-null mutant embryos as we listed mARID3b as a gene whose expression pattern is similar to PDGFRα (Soriano, 1997). In fact, mARID3b expression overlaps with that of PDGFRα in both cranial mesenchymal and caudal mesodermal regions including nascent somites (Takakura et al., 1997). It is therefore plausible to suggest that PDGFRα and mARID3b are directly interacting with each other during the development of PDGFRα$^+$ cells. However, as expression of mARID3b and PDGFRα is maintained by null mutation of PDGFRα and mARID3b genes, respectively,

it is more likely that the two molecules are involved in independent processes. Consistent with this view is a previous report on cranial mesenchyme specific conditional knockout of PDGFRα, showing that PDGFRα is involved in differentiation of cranial mesenchymal cells rather than their survival (Tallquist and Soriano, 2003). In contrast to this, mARID3b's role in cranial mesenchymal cells is to prevent their apoptosis.

One of the most conspicuous phenotypes of mARID3b-null mutants is a defect in the development of the cardiovascular system. However, mARID3b expression was undetectable both in cardiac muscle and blood vessels during all stages of embryogenesis. Moreover, endothelial cells, as well as cardiac muscles, can differentiate in the mutant embryos. It is likely that mARID3b does not play a cell-autonomous role in differentiation of endothelial and cardiac muscle cells. Concerning the cardiovascular phenotype, we found that mARID3b-null embryos show a marked resemblance to dHand-null mutant embryos (Srivastava et al., 1997; Thomas et al., 1998). While dHand was shown to have a direct role in the formation of ventricular muscles, the defect of heart formation in dHand-null mutant is mainly due to branchial arch growth failure from apoptosis. The fact that growth of branchial arch cells is severely impaired by apoptosis in mARID3b-null mutant embryos leads us to speculate that the cellular process causing cardiac defect of the mARID3b-null mutant mouse is due to a failure in recruiting cranial mesenchymal cells. As heart function is required for vascular remodeling, circulation defects may account for the majority of defects in vascular remodeling. The reduction in cranial mesenchyme production may also account for the occlusion of the dorsal aorta and cardinal vein as mesoderm and cranial mesenchyme are known to migrate to remote sites and are involved in formation of various tissues. Although the phenotype of KO embryos appears to be complicated in initial observations, we speculate that the cellular processes responsible for the major phenotypes of mARID3b-null mutant mice can be simply ascribed to the failure in recruiting cranial mesenchymal cells to the area where they migrate.

This study shows that enhanced apoptosis is the major cellular basis for the defect of growth of cranial mesenchymal cells in mARID3b-null mutants. hARID3A, the closest member to hARID3B, acts as a positive regulator of cell proliferation. Over expression of this molecule can immortalize mouse embryonic fibroblasts (MEF) through bypassing the H-RAS^{V12}-induced senescence (Peeper et al., 2002). As the DNA binding domain of hARID3A, which is essential for ARID family function (Wilsker et al., 2002), is very similar to that of mARID3b, it is plausible that mARID3b acts in a similar manner to hARID3A in cranial mesenchymal cells. Our observation that their growth is impaired from massive cell death is consistent with this possibility. During embryogenesis, there are numerous situations in which a large number of a particular cell type need to be prepared in a short period of time. While induction of cell proliferation is usually mediated by external signals, strong growth signals are often associated with cell senescence. We speculate that transient expression of senescence bypassing

mechanisms, such as mARID3b, according to a developmental program is a common mechanism for expanding a particular population.

This study shows that the mARID3b molecule is indispensable for the production of cranial mesenchymal tissues. As studies of ARID family molecules in mammalian embryogenesis are still limited, our present report has the potential to shed new light on novel molecular mechanisms regulating the production of proper amounts of cells.

Acknowledgments

Appendix A. Supplementary data

Supplementary data associated with this article can be found in the online version at doi:10.1016/j.ydbio.2005.12.016.

References

Anderson, K.V., Ingham, P.W., 2003. The transformation of the model organism: a decade of developmental genetics. Nat. Genet. 33, 285–293.

Araki, K., Imaizumi, T., Okuyama, K., Oike, Y., Yamamura, K., 1997. Efficiency of recombination by Cre transient expression in embryonic stem cells: comparison of various promoters. J. Biochem. 122, 977–982.

Aubert, J., Dunstan, H., Chambers, I., Smith, A., 2002. Functional gene screening in embryonic stem cells implicates Wnt antagonism in neural differentiation. Nat. Biotechnol. 20, 1240–1245.

Chen, E., Ekker, S.C., 2004. Zebrafish as a genomics research model. Curr. Pharm. Biotechnol. 5, 409–413.

Debouck, C., Goodfellow, P.N., 1999. DNA microarrays in drug discovery and development. Nat. Genet. 21, 48–50.

Era, T., Witte, O.N., 2000. Regulated expression of P210 Bcr-Abl during embryonic stem cell differentiation stimulates multipotential progenitor expansion and myeloid cell fate. Proc. Natl. Acad. Sci. U. S. A. 97, 1737–1742.

Gehring, W.J., 1993. Exploring the homeobox. Gene 135, 215–221.

Iwahara, J., Iwahara, M., Daughdrill, G.W., Ford, J., Clubb, R.T., 2002. The structure of the Dead ringer–DNA complex reveals how AT-rich interaction domains (ARIDs) recognize DNA. EMBO J. 21, 1197–1209.

Jackson, M., Baird, J.W., Cambray, N., Ansell, J.D., Forrester, L.M., Graham, G.J., 2002. Cloning and characterization of Ehox, a novel homeobox gene essential for embryonic stem cell differentiation. J. Biol. Chem. 277, 38683–38692.

Kabrun, N., Buhring, H.J., Choi, K., Ullrich, A., Risau, W., Keller, G., 1997. Flk-1 expression defines a population of early embryonic hematopoietic precursors. Development 124, 2039–2048.

Kataoka, H., Takakura, N., Nishikawa, S., Tsuchida, K., Kodama, H., Kunisada, T., Risau, W., Kita, T., Nishikawa, S.I., 1997. Expressions of PDGF receptor alpha, c-Kit and Flk1 genes clustering in mouse chromosome 5 define distinct subsets of nascent mesodermal cells. Dev. Growth Differ. 39, 729–740.

Kortschak, R.D., Tucker, P.W., Saint, R., 2000. ARID proteins come in from the desert. Trends Biochem. Sci. 25, 294–299.

Loebel, D.A., Watson, C.M., De Young, R.A., Tam, P.P., 2003. Lineage choice and differentiation in mouse embryos and embryonic stem cells. Dev. Biol. 264, 1–14.

Nakayama, N., Duryea, D., Manoukian, R., Chow, G., Han, C.Y., 2003. Macroscopic cartilage formation with embryonic stem-cell-derived mesodermal progenitor cells. J. Cell Sci. 116, 2015–2028.

Nishikawa, S.I., Nishikawa, S., Hirashima, M., Matsuyoshi, N., Kodama, H., 1998. Progressive lineage analysis by cell sorting and culture identifies FLK1+VE-cadherin+ cells at a diverging point of endothelial and hematopoietic lineages. Development 125, 1747–1757.

Numata, S., Claudio, P.P., Dean, C., Giordano, A., Croce, C.M., 1999. Bdp, a new member of a family of DNA-binding proteins, associates with the retinoblastoma gene product. Cancer Res. 59, 3741–3747.

Peeper, D.S., Shvarts, A., Brummelkamp, T., Douma, S., Koh, E.Y., Daley, G.Q., Bernards, R., 2002. A functional screen identifies hDRIL1 as an oncogene that rescues RAS-induced senescence. Nat. Cell Biol. 4, 148–153.

Sakurai, H., Era, T., Jakt, L.M., Okada, M., Nagai, S., Nishikawa, S., Nishikawa, S.-I., in press. In vitro modeling of paraxial and lateral mesoderm differentiation reveals early reversibility. Stem Cells.

Schatteman, G.C., Morrison-Graham, K., van Koppen, A., Weston, J.A., Bowen-Pope, D.F., 1992. Regulation and role of PDGF receptor alpha-subunit expression during embryogenesis. Development 115, 123–131.

Shandala, T., Kortschak, R.D., Gregory, S., Saint, R., 1999. The Drosophila dead ringer gene is required for early embryonic patterning through regulation of argos and buttonhead expression. Development 126, 4341–4349.

Smith, L., Greenfield, A., 2003. DNA microarrays and development. Hum. Mol. Genet. 2 (1), R1–R8.

Soriano, P., 1997. The PDGF alpha receptor is required for neural crest cell development and for normal patterning of the somites. Development 124, 2691–2700.

Srivastava, D., Thomas, T., Lin, Q., Kirby, M.L., Brown, D., Olson, E.N., 1997. Regulation of cardiac mesodermal and neural crest development by the bHLH transcription factor, dHAND. Nat. Genet. 16, 154–160.

Stephenson, D.A., Mercola, M., Anderson, E., Wang, C.Y., Stiles, C.D., Bowen-Pope, D.F., Chapman, V.M., 1991. Platelet-derived growth factor receptor alpha-subunit gene (Pdgfra) is deleted in the mouse patch (Ph) mutation. Proc. Natl. Acad. Sci. U. S. A. 88, 6–10.

Takakura, N., Yoshida, H., Kunisada, T., Nishikawa, S., Nishikawa, S.I., 1996. Involvement of platelet-derived growth factor receptor-alpha in hair canal formation. J. Invest. Dermatol. 107, 770–777.

Takakura, N., Yoshida, H., Ogura, Y., Kataoka, H., Nishikawa, S., 1997. PDGFR alpha expression during mouse embryogenesis: immunolocalization analyzed by whole-mount immunohistostaining using the monoclonal anti-mouse PDGFR alpha antibody APA5. J. Histochem. Cytochem. 45, 883–893.

Tallquist, M.D., Soriano, P., 2003. Cell autonomous requirement for PDGFRalpha in populations of cranial and cardiac neural crest cells. Development 130, 507–518.

Thomas, T., Kurihara, H., Yamagishi, H., Kurihara, Y., Yazaki, Y., Olson, E.N., Srivastava, D., 1998. A signaling cascade involving endothelin-1, dHAND and msx1 regulates development of neural-crest-derived branchial arch mesenchyme. Development 125, 3005–3014.

Wang, L., Li, L., Shojaei, F., Levac, K., Cerdan, C., Menendez, P., Martin, T., Rouleau, A., Bhatia, M., 2004. Endothelial and hematopoietic cell fate of human embryonic stem cells originates from primitive endothelium with hemangioblastic properties. Immunity 21, 31–41.

Weinberg, R.A., 1991. Tumor suppressor genes. Science 254, 1138–1146.

Weston, J.A., Yoshida, H., Robinson, V., Nishikawa, S., Fraser, S.T., 2004. Neural crest and the origin of ectomesenchyme: neural fold heterogeneity suggests an alternative hypothesis. Dev. Dyn. 229, 118–130.

Wilsker, D., Patsialou, A., Dallas, P.B., Moran, E., 2002. ARID proteins: a diverse family of DNA binding proteins implicated in the control of cell growth, differentiation, and development. Cell Growth Differ. 13, 95–106.

Yagi, T., Tokunaga, T., Furuta, Y., Nada, S., Yoshida, M., Tsukada, T.,

Saga, Y., Takeda, N., Ikawa, Y., Aizawa, S., 1993. A novel ES cell line, TT2, with high germline-differentiating potency. Anal. Biochem. 214, 70–76.

Yamaguchi, T.P., Dumont, D.J., Conlon, R.A., Breitman, M.L., Rossant, J., 1993. flk-1, an flt-related receptor tyrosine kinase is an early marker for endothelial cell precursors. Development 118, 489–498.

Yamashita, J., Itoh, H., Hirashima, M., Ogawa, M., Nishikawa, S., Yurugi, T., Naito, M., Nakao, K., 2000. Flk1-positive cells derived from embryonic stem cells serve as vascular progenitors. Nature 408, 92–96.

Zhang, X.Q., Afink, G.B., Svensson, K., Jacobs, J.J., Gunther, T., Forsberg-Nilsson, K., van Zoelen, E.J., Westermark, B., Nister, M., 1998. Specific expression in mouse mesoderm- and neural crest-derived tissues of a human PDGFRA promoter/lacZ transgene. Mech. Dev. 70, 167–180.